geosciences

MDPI

Article

Understanding Sediment Dynamics at a Shipwreck Site Using CFD Modelling

Gary Littler [1,2], Mark Coughlan [1,2,3], Jan Majcher [4] and Jennifer Keenahan [1,*]

[1] School of Civil Engineering, University College Dublin, Belfield, D04 V1W8 Dublin, Ireland
[2] Gavin and Doherty Geosolutions, Unit A2, Nutgrove Office Park Rathfarnham, Dublin 14, D14 X627 Dublin, Ireland
[3] SFI Centre for Research in Applied Geosciences (iCRAG), O'Brien Centre for Science East, University College Dublin, D04 V1W8 Dublin, Ireland
[4] School of Geography and Environmental Sciences, University of Ulster, Coleraine BT52 1SA, Northern Ireland, UK
* Correspondence: jennifer.keenahan@ucd.ie

Abstract: Shipwrecks are important cultural heritage sites offshore. In many instances, given their often long-term emplacement on the seafloor, they offer natural laboratories to study complex interactions between human-induced obstacles and seabed dynamics. Such interactions and induced sediment mobility also pose significant threats to offshore engineering infrastructure, such as turbine monopile foundations. Traditional methods can struggle to capture the nuance of these processes, with real-world surveys measuring effects only after installation, and laboratory models suffering from scale-down inaccuracies. Computational fluid dynamics (CFD) modelling offers an effective means of investigating the effects of obstacles on seabed dynamics, and by using shipwrecks as proxies for infrastructure, it can utilize long-term datasets to verify its predictions. In this study, high-resolution temporal bathymetric data were used in, and to verify, CFD modelling to investigate the interactions between hydro- and sediment dynamics at a shipwreck site in a tidally dominated wreck site. From this comparison, simulations of bed shear stress and scalar transport correlate well with known areas of erosion and deposition, serving as a basis for future scour prediction studies and creating effective tools in offshore renewable infrastructure planning and de-risking.

Keywords: scour; morphodynamics; hydrodynamics; CFD modelling; shipwrecks; offshore wind

Citation: Littler, G.; Coughlan, M.; Majcher, J.; Keenahan, J. Understanding Sediment Dynamics at a Shipwreck Site Using CFD Modelling. *Geosciences* **2022**, *12*, 369. https://doi.org/10.3390/geosciences12100369

Academic Editors: Angelo Aloisio, Said Quqa, Pier Francesco Giordano, Luke J. Prendergast and Jesus Martinez-Frias

Received: 29 July 2022
Accepted: 2 October 2022
Published: 7 October 2022

1. Introduction

Shipwrecks on the seabed are generally avoided in terms of offshore wind development as they are protected locations of high cultural heritage value. However, increasingly they are being used as natural laboratories on the seabed to study the complex interaction of man-made objects, seafloor sediment transport and hydrodynamic processes [1]. Offshore wind is seen as a critical technology towards decarbonizing electricity demand. When it comes to siting individual turbines on the seafloor, the issue of seabed mobility and the potential for scour development is a significant geohazard and environmental constraint associated with the development of this sector, as well as other engineering infrastructure such as pipelines and cables [2]. Scour is the process in which sediment is eroded and transported due to an imposed shear stress generated by seabed current and/or waves. Its effects have been widely reported, documented, and examined [3–5]. The rate of erosion is largely dependent on the energy generated by local flow regimes and the properties of the sediment at the seafloor.

Whilst scour is a naturally occurring phenomenon, the introduction of obstacles into a system can magnify the effects due to an increase in bed shear stress caused by fluid flowing around the obstacle creating pressure differences, increased flow velocity and turbulence [6,7]. Over time, this can lead to the formation of scour holes around the

obstacle where the shear stress is highest, and deposition as the energy and turbidity of the flow decreases to the point the suspended sediment can no longer be transported in the water column. These scour holes can lead to damage and destabilization of structures such as turbine foundations and "free-spanning" of cables, requiring concerted efforts to remediate existing damage and prevent further scour occurring. Mitigating defenses such as rock armor can be utilized after initial installation, and have been extensively examined [8–12]. These can be technically difficult to implement however, making them financially costly when installed after scour has occurred or placed in anticipation of possible issues. Ireland's only offshore wind farm constructed to date, Arklow Bank, experienced scour issues that had a significant impact on the project resulting in the use of rock armor in an attempt to mitigate against further scour and turbine instability [13]. Therefore, pre-empting such issues and identifying the optimum area for placement of defenses, or avoiding areas of high shear stress altogether, can increase the viability and longevity of installations. Based on experiences across Europe, there is a significant amount of focus on geotechnical assessments for scour and related processes in relation to offshore engineering and mitigation [11]. Efforts to predict sediment dynamics and scour evolution can be challenging, as in situ measurements and observations involve using remote sensing techniques with visual interpretation of the seabed features [3] without examining current flow dynamics. These methods can be costly, time-consuming, and provide an incomplete understanding of the forces at work due to the large scale of the task. Other methods include small laboratory-based modelling [5], larger models contained in specialized facilities [14] or specialized full-scale experiments such as that performed by Ma and Chen [9] on the National Renewable Energy Laboratory (NREL) wind turbine in the U.S. There are, however, significant limitations imposed on these methods. Scaling down models introduces unavoidable errors due to the loss of real-world variables. Full-scale test models still suffer from difficulty recording measurements, although to a lesser extent than their real-world counterparts, and conditions such as the weather can hinder prospective studies. In general, there is a clear need for a better understanding of localized seabed dynamics and subsequent impacts on morphodynamics and scour development. However, there is a paucity of direct observations and data on scour development processes.

Computational fluid dynamics (CFD) is a tool that can be used to model the current flow dynamics of a section of the seabed, along with any obstacles or obstructions contained within the area. Therefore, the application of CFD modelling is further enhancing the understanding of hydrodynamic processes driving sediment transport and scour [15]. Using a solver based on Navier–Stokes equations, fluid flow can be simulated and its interaction with obstacles analyzed. Smyth and Quinn [16], Quinn and Smyth [17], and Fernández-Montblanc et al. [18] demonstrated how CFD modelling applied over a shipwreck site could garner significant insight into the hydrodynamic regime, including interaction with seafloor sediments, in understanding scour signature formation processes. When combined with repeat hydrographic surveys that provide high-resolution bathymetric data detailing seabed geomorphic change, CFD is a powerful tool to elucidate patterns of turbulent flow and enhanced currents around seabed obstructions at a localized scale. Turbulence models can also be utilized to increase the accuracy of the model in complex systems, allowing for more detailed analyses of the flow. By using an approach based on CFD, it is possible to produce an accurate and cost-effective prediction model for scour on a large spatial scale without the complexities of in situ modelling. For example, Yang et al., [19] utilized the commercial CFD software ANSYS Fluent in order to determine the effectiveness of a submerged tidal current turbine (TCT) for scour mitigation and extra green energy production. CFD enabled the identification of a need for the correct positioning of the TCT at the base of the monopile for optimum performance. When used in conjunction with real-world measurements, its effectiveness can be increased even further through verification and validation.

The ability to accurately predict and quantify areas of high shear stress potentially occurring around structures using real-world conditions such as flow velocity, turbulence,

and sediment type, can help inform the planning of installations with regard to location, engineering and design. When these conditions are taken into consideration, mitigation methods could be better adapted to suit the specific area identified at an early stage in the development process. However, these models require some degree of validation to verify outputs. Shipwrecks offer novel in situ features with which to test theories of hydrodynamics and sediment transport around seabed objects, with CFD modelling offering a robust tool to do so. The aim of this paper is to use a CFD model developed for a shipwreck site in the Irish Sea in order to better understand hydro- and sediment dynamics, which can then be applied to de-risking offshore infrastructure planning, specifically wind turbine foundations. These shipwrecks provide a proxy for long-term measurement of sediment dynamics and flow regimes, as some WW1 wrecks have been around for over 100 years and have been surveyed extensively as they are sites of archaeological and cultural importance. Irish wind farm development is still in its infancy, however, with long-term data for sediment behavior around these installations unavailable. By simulating current flow patterns and magnitudes, it is possible to better constrain and predict seabed morphological patterns of sediment erosion and deposition caused by obstructions on the seabed. By integrating a scalar transport model into an OpenFOAM solver such as SimpleFOAM, it is possible to examine the sediment transport potential in the flows around the wreck in addition to flow patterns and shear stress. This novel approach, when combined with other high-resolution seabed survey data, could potentially be applied to critical offshore engineering as a basis for building a robust methodology to assess the impacts of sediment dynamics and prevent scour and other adverse impacts from mobile sediment at the seafloor.

2. Description of the Site

The SS Polwell is located approximately 10 km off the east coast of Ireland, north of Dublin, in the Irish Sea (Figure 1). It originally measured 86.56 × 11.6 × 5.53 meters and operated as a defensively armed steam collier. It was torpedoed by a German submarine on 5 June 1918 with no loss of life. The wreck lies in approximately 30 m water depth, orientated NE-SW with the bow to the NE, on seabed comprising a multimodal distribution of sediment types [1]. Ground-truthing grab samples taken from the site suggest muddy sand and slightly gravelly muddy sand. To the south of the SS Polwell are a number of seabed ridges believed to be out-cropping bedrock or glacial till. Approximately 600 m to the north of the SS Polwell site, a gas interconnector pipeline transverses east–west. Previous residual relief modelling highlighted extensive erosional and depositional features to the north of the site, with limited development to the south due to the presence of the seabed ridges [20]. Modelled data for seabed currents in the area suggest a dominant NW-SE direction of flow reaching a maximum of 0.4 m/s.

This shipwreck has already been investigated as part of other studies [1,20]. Repeated high-resolution bathymetric data have been collected at the SS Polwell site onboard the RV Celtic Voyager as part of three separate surveys in 2015 (CV15021), 2016 (CV16031) and 2019 (CV19026) under the Marine Institute Ship-Time Programme, allowing for detailed and general site characterization. In this study, bathymetric data collected as part of the CV19026 survey were used. The multibeam echosounder (MBES) data were acquired using a dual-head, hull-mounted Kongsberg EM2040 operating at 400 kHz, with a continuous wave pulse. An integrated Global Navigation Satellite System (GNSS)/L-Band receiver Civil Navigation (CNAV) 3050 provided primary position corrections, and a Seatex Seapath 330+ acted as a secondary positioning system as well as providing motion referencing and timing. Survey lines were aligned in a grid, which allowed for 110–120° swath coverage. Data from the 2019 survey were cleaned and processed in Caris Hydrographic Information Processing System and Sonar Information Processing System (HIPS and SIPS) v. 9 using the Combined Uncertainty and Bathymetry Estimator algorithm [21] and were tidally corrected before being exported as digital elevation models (DEMs) as raster format in the Universal Transverse Mercator (UTM) 30N projection. The horizontal resolution of this dataset is

0.2 m. More details on all data processing and compliance with International Hydrographic Organisation (IHO) Special Order standards can be found in [1,20]. DEM rasters were used as geometry input for CFD modelling efforts.

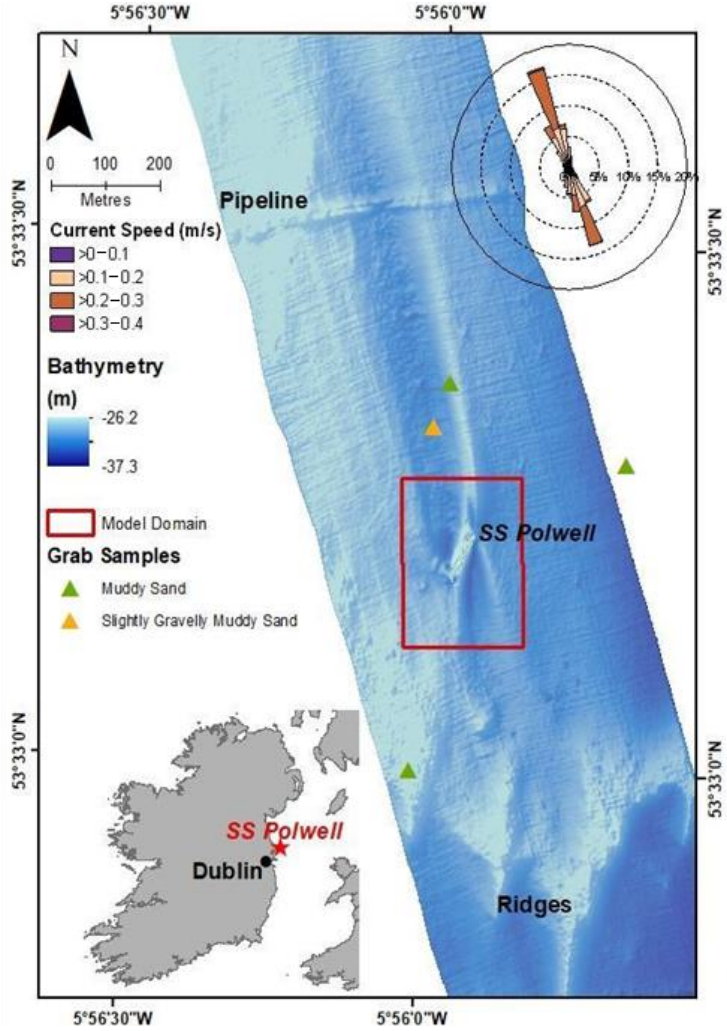

Figure 1. Location of the SS Polwell in the Irish Sea and site characterization. Rose chart (top right) represents modelled data for near-seabed currents. Bathymetry data is presented with a hillshade effect (azimuth 315°, elevation 45°). Model domain presented in this study is highlighted by the red box. Grab sample locations are represented by colored triangles.

3. CFD Model

3.1. Underlying Physics and Simplifications

The modelling approach adopted in this study was to use a single-phase fluid solver. No coupling with a morphological model or bed deformations is included as part of this study. The SS Polwell lies in a mix of muddy sand and slightly gravelly muddy sand, which has been modelled here as rippled sand by generating a surface to represent the seabed and applying a roughness value corresponding to a sediment grain size median of d50. Majcher et al. [1,22] determined exceedance values for shear stress on sediment types around a wreck, a critical value where, when exceeded, sediment mobilization takes place from the seabed. This study was concerned with the transport of suspended material after mobilization has taken place, exceedance values were not explored as grab samples were taken for the area surrounding the SS Polwell, but not in the direct vicinity of the wreck itself. Transport calculations were based on a dimensionless value applied to a proxy tracer using ScalarTransportFoam, specific particle values were not applied. The

effects of landforms and artificial obstacles outside the study area on the inlet flows were not considered. The seawater properties in the model, such as density, were based on a temperature of 10 °C across the study area. The effects of hydrostatic pressure were excluded from this study. Current velocity magnitudes were based on depth averaged readings from the Marine Institute of Ireland's implementation of the Regional Oceanic Modelling System (ROMS). These were used to calculate and provide inlet velocity profiles. The two modelled flow directions were based on a dominant NW to SE tidal flow, derived from a mean of directional values between 270 and 360 degrees, and secondary SE to NW flow on tidal reversal. The turbulent flow was solved using Reynolds Averaged Navier–Stokes (RANS) equations, a time averaged version of the Navier–Stokes equations.

3.2. Governing Equations

In the presented CFD model, the flow within the testing domain is assumed to be incompressible, Newtonian, and statistically stationary, with temperature effects neglected. the flow is governed by the Reynolds-Averaged Navier–Stokes (RANS) formulation for mass and momentum:

$$\begin{aligned} &\nabla \cdot U = 0 \\ &\nabla \cdot (UU) = \nabla \cdot [\nu_{eff} \, (\nabla U + (\nabla U)^T)] - \nabla p \end{aligned} \tag{1}$$

where U is the time-averaged velocity, p is the time-averaged kinematic pressure (pressure divided by density), and ν_{eff} is the effective kinematic viscosity, which is the summation of laminar kinematic viscosity (ν) and the turbulent kinematic viscosity (ν_t). The value of ν is 1.307×10^{-6} m^2/s, representing water at (10 °C). The unknown ν_t is calculated from the turbulence kinetic energy (k) and the energy dissipation frequency (ω) using the k-ω SST (shear stress transport) turbulence model due to its ability to solve, in detail, at both the boundaries and the internal field. As the study area was considered quite large, the k-ω SST model was deemed more suitable than other models to provide an accurate calculation of shear stress at the seabed, in addition to flow in the water column. This approach has been used by Yu and Thé [23] to model pollution dispersal in a large urban environment.

In this study, the RANS simulations employ the SIMPLE algorithm to perform pressure–velocity coupling (simpleFOAM solver in OpenFOAM-v2012). It is the steady-state solver for incompressible, turbulent flow. In addition, a passive scalar transport model was integrated into the simpleFOAM solver:

$$\frac{\partial T}{\partial t} + \nabla \ (UT) - \nabla^2 \, (D_T T) = 0 \tag{2}$$

where T is the transported scalar, U is the fluid velocity, and D_T is the diffusion coefficient divided by the fluid density, with both assumed to be constant. This passive scalar represents the transport of sediment of undefined characteristics, after mobilization has taken place. It has no dynamical effect on the fluid flow itself.

3.3. Geometry

The geometry of the seabed and wreck of the SS Polwell for CFD simulations were constructed from digital elevation models and point cloud files derived from multibeam echosounder bathymetry data. These data were gathered as part of the 2019 GIST Survey (CV19026) under the Marine Institute Ship-Time Programme, at a resolution of 0.2 m. This file was then converted into a stereolithography (.stl) file to provide a 3-dimensional representation, as well as compatibility with OpenFOAM v_2012. In order to accurately represent the correct flow direction, the .stl file was rotated in Blender version 2.92.0 to align with the dominant north-westerly flow. This was repeated for the south-easterly current direction to provide an accurate representation of flow in a predominately bidirectional system. A final file was generated that covered an area of seabed approximately 130 m wide by 180 m long, with the direction of the longer sides perpendicular to the inlet boundary. The geometry was placed at point 0 on the z axis of the domain, 10 m above the base

of the mesh to avoid interference where the dips in the seabed would cross outside the computational domain. The seabed and wreck geometry were prescribed a predefined roughness length (Z_0) of 0.06 m, representing rippled sand, as used by [15].

3.4. Computational Domain and Boundary Conditions

Best practice guidance on domain size by Franke et al. [24] suggests the domain should be based on the height and lateral extension of the obstacle involved. Mo et al. [25] further expand on this for the flow of wind turbines. Although the subjects of these studies differ from the model included in this paper in that they are concerned with the flow of air as opposed to sea water, the overarching point remains valid: the domain size is relative to the dimensions of the object of the study. The cuboidal computational domain in this study represents a length of 100 m, a width of 100 m and a depth of 35 m. The actual domain descends a further 10 m vertically from the 3D geometry, which is situated at 0 m, giving a Y axis value of −10 m to +25 m. This was required as the natural undulations on the seabed caused it to dip below 0m, exposing the base of the mesh and introducing interference into the model. Although Franke et al. [24] suggests vertical extension at five times the height of the object, our model is limited by the depth of the wreck. The SS Polwell lies at a depth of 29.8 m; however, the surface of the sea is a dynamic and changing environment. The 4.8 m excluded from the natural domain provides a buffer where tidal and wave induced influences might occur. At much greater depths, the main concern would have been balancing computational power required with an adequate vertical study zone allowing full evolution of the flow. Mo et al. [25] concluded that a computational domain size that is not large enough limits the full development of the flow.

This paper aimed to examine scour induced by flow around the wreck by highlighting zones of high shear stress. In this study, the area of seabed immediately adjacent to the shipwreck site of the SS Polwell was considered due to the fine-scale construction of the simulation domain and constraints on computing capacity in terms of runtime. The two areas most vital to this study were the approach flow and the wake of the SS Polwell. Therefore, the extension of the seabed provided by the bathymetric data was deemed adequate for the model.

The boundary domain (Figure 2) consisted of six faces, with fluid flow moving from the inlet to the outlet. Inlet and outlet boundary conditions were created at opposite sides to define a flow direction, with the geometry oriented to represent the prevailing current. The patch types assigned to each of the six faces are shown in Table 1.

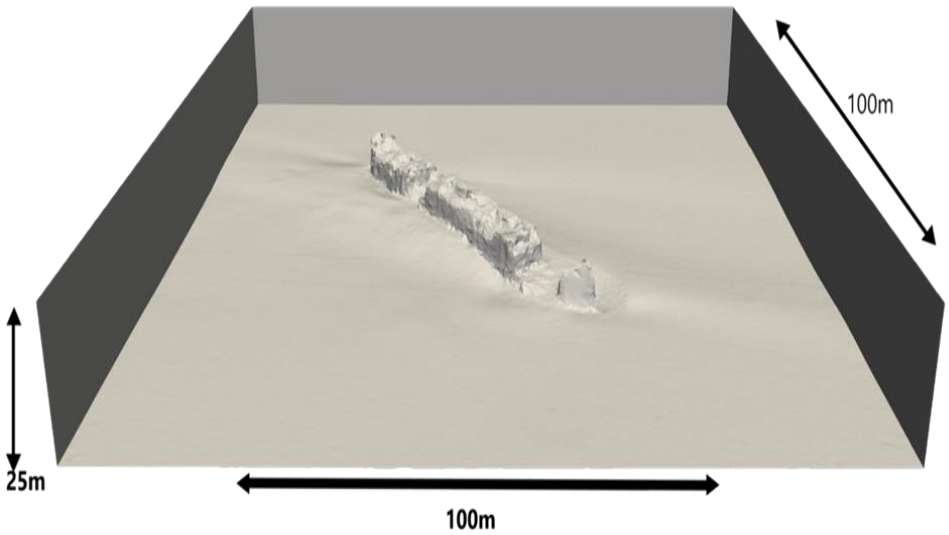

Figure 2. Computational domain for the SS Polwell.

Table 1. Setup of patch types for boundaries in blockmesh.

BlockMesh Boundary Face	Patch Type
Inlet	Patch
Outlet	Patch
Top	Slip
Bottom	Wall
Front/Back	Symmetry Plane

A power-law velocity profile was generated at the inlet for U by using the equation described in [26,27]:

$$U(z) = \left(\frac{z}{0.32h}\right)^{1/7} \underline{U} \quad (3)$$

where the velocity profile (the velocity at height z above the seabed $U_{(z)}$) is described using a power law (α) and bed roughness coefficient (β), with water depth (h) and depth averaged velocity ($\bar{U}$, 0.147 m/s at 1m from the seabed). Current data for the SS Polwell were obtained from the Marine Institute of Ireland using output from their operational hydrodynamic model [27], which is run on the Regional Ocean Modelling System (ROMS: [28,29]). Data were obtained for depth-averaged current velocity and direction for a 1-year period and were used in site characterization (see current speed rose Figure 1) and as inlet current speed values in CFD modelling efforts. Values were generated using the above formula and entered into a .csv file for use with the OpenFOAM fixedProfile boundary condition.

A summary of the boundary conditions of the five primary unknowns (U, p, k and ω and nut) applied at each boundary region is shown in Table 2.

Table 2. Boundary conditions of simulations based on the k-ω SST model.

	P	U	K	ω	NUT	T
Dimensions (mass, length, time, temperature, quantity, current, luminous intensity)	[0 2 −2 0 0 0 0]	[0 1 −1 0 0 0 0]	[0 2 −2 0 0 0 0]	[0 0 −1 0 0 0 0]	[0 2 −1 0 0 0 0]	[0 0 0 1 0 0 0]
Units	m^2/s^2	m/s	m^2/s^2	s^{-1}	m^2/s^{-1}	Dimensionless
Internalfield SS Powell	Uniform 0	Uniform (0 0 0)	Uniform 0.000013	Uniform 0.00206	Uniform 0	Uniform 0
Internalfield SS Hare	Uniform 0	Uniform (0 0 0)	Uniform 0.00003174	Uniform 0.00123	Uniform 0	Uniform 0
Inlet	Zero gradient	Fixed profile	Fixed value; Value $ Internalfield;	Fixed value; Value Uniform 1	Calculated; Value Uniform 0	Fixed value; Value Uniform 1
Outlet	Fixed value; Value Uniform 0	Zero gradient	Inletoutlet; Inletvalue $ Internalfield; Value $ Internalfield	Inletoutlet; Inletvalue $ Internalfield; Value $ Internalfield	Zero gradient	Zero gradient
Top	Slip	Slip	Slip	Slip	Slip	Slip
Bottom	Zero gradient	Zero gradient	KQR wall function Value $ Internalfield	Zero gradient	NUT wall function Value Uniform 0	Zero gradient

Table 2. *Cont.*

	P	U	K	ω	NUT	T
Front/Back	Symmetry plane	Symmetry plane	Symmetry plane	Symmetry plane	Symmetry plane	Symmetry plane
Polwell/ Hare (Patch applied to seabed and wreck geometry)	Zero gradient	No Slip	KQR wall function Value $ Internalfield	Omega wall function value $ Internalfield	NUT wall function Ks Uniform 0.000755; Cs Uniform 0.5 Value Uniform 0	Zero gradient

3.5. Computational Mesh

The computational mesh used in the simulations was created using OpenFOAM utilities snappyHexMesh and blockMesh (Figure 3). It is a hybrid mesh containing a structured background grid and an unstructured hexahedron-dominated mesh in the near-wall region. Each blockMesh cell was assigned a uniform size of 2 m × 1 m × 2 m in all directions, with the geometry positioned at 0m on the Y axis. SnappyHexMesh was used to generate, position and refine the seabed and shipwreck geometry.

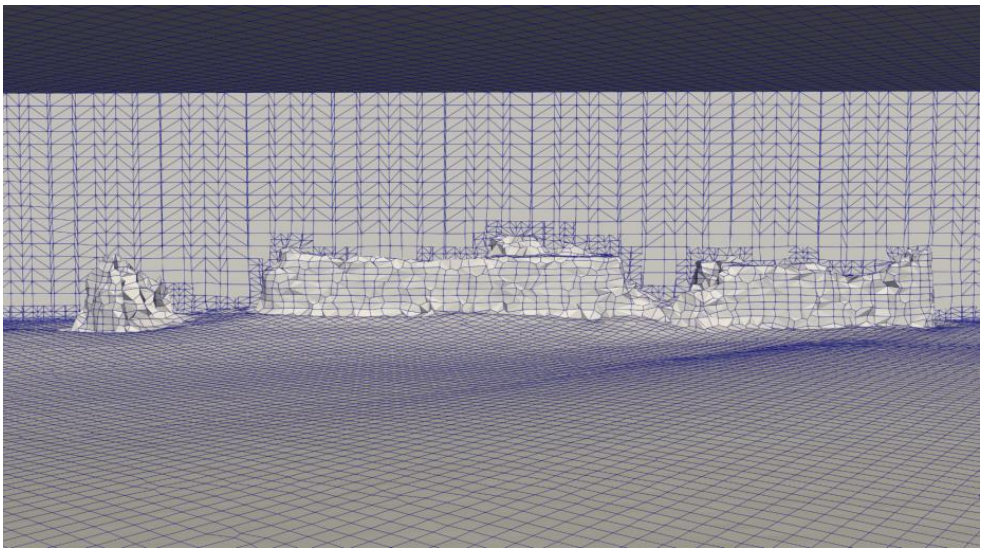

Figure 3. Computational mesh including boundary cells and 3D geometry mesh.

A mesh sensitivity study was performed, starting with a coarse mesh and gradually increasing the fineness of the mesh by reducing cell sizes, until mesh independence was achieved. The mesh was considered adequate when computational time was reduced to its minimum, while maintaining a suitable level of detail. Simulations were performed with 219,741 cells, 264,093 cells, and 342,091 cells. The results displayed no significant change (~1%) in the mean values for the time-averaged velocity, U, between the two finest meshes (Table 3).

Table 3. Results of mesh sensitivity study. Note in the final column change is measured relative to Mesh no. 2.

Mesh	No. of Cells	U Mean (m/s)	Change
1	219,741	0.091764943	−1.27%
2	264,093	0.090614409	-
3	342,091	0.089529869	1.20%

The mesh with 264,093 cells was chosen due to the lower computational demand with minimal change in values of velocity. This consisted of three defined layers and an expansion ratio of 1.4. The model was considered converged at around 1700 iterations based on the calculation of the residual of a single vector component; in this instance, U_x (direction of inlet to outlet) (Figure 4), with the value remaining constant below 10^{-4}. The other vectors comprise $U_{y,}$ the direction of bottom to top, and U_z, the direction of model front to back. The simulations were allowed to run for up to 10,000 iterations to confirm that the residuals remained constant beyond 3000 iterations.

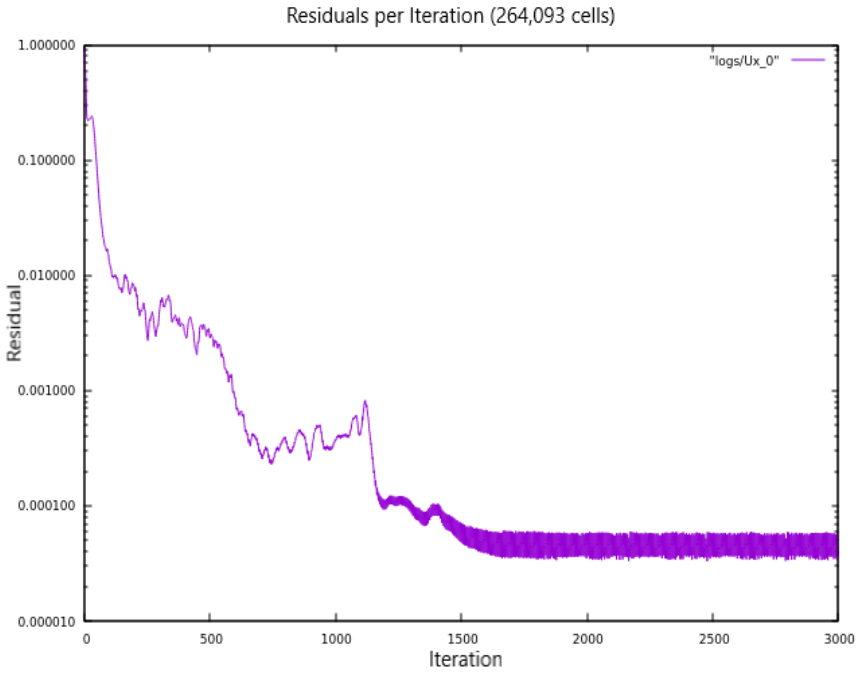

Figure 4. Graph showing the evolution of residual values for *Ux*, on the NW to SE flow model, from 0 to 3000 iterations. Model had an overall cell value of 264,093.

This shipwreck has already been investigated as part of other studies [1].

4. Results

CFD model outputs for flow velocity, flow patterns and bed shear stress were visualized and analyzed in ArcMap version 10.7 and Paraview version 5.9.0. Analysis was carried out on results from two separate simulations representing the dominant flow directions: from NW to SE and SE to NW. Given the lack of in situ measurement data from this site, it was not possible to perform a full validation. Instead, model output results were compared with known seabed geomorphological changes associated with erosion and deposition as calculated by Majcher et al. [1] from temporal analysis of bathymetry data for verification.

4.1. Flow Velocity and Patterns

Bed flow velocity values were derived from the cells immediately adjacent to the seabed. Figure 5 shows a maximum velocity value of 0.26 m/s and a minimum value of

0.001 m/s for the NW to SE flow and a maximum of 0.25 m/s and a minimum of 0.006 for the SE flow. The mean current speed for the NE was 0.09 m/s, and 0.08 m/s for the SE.

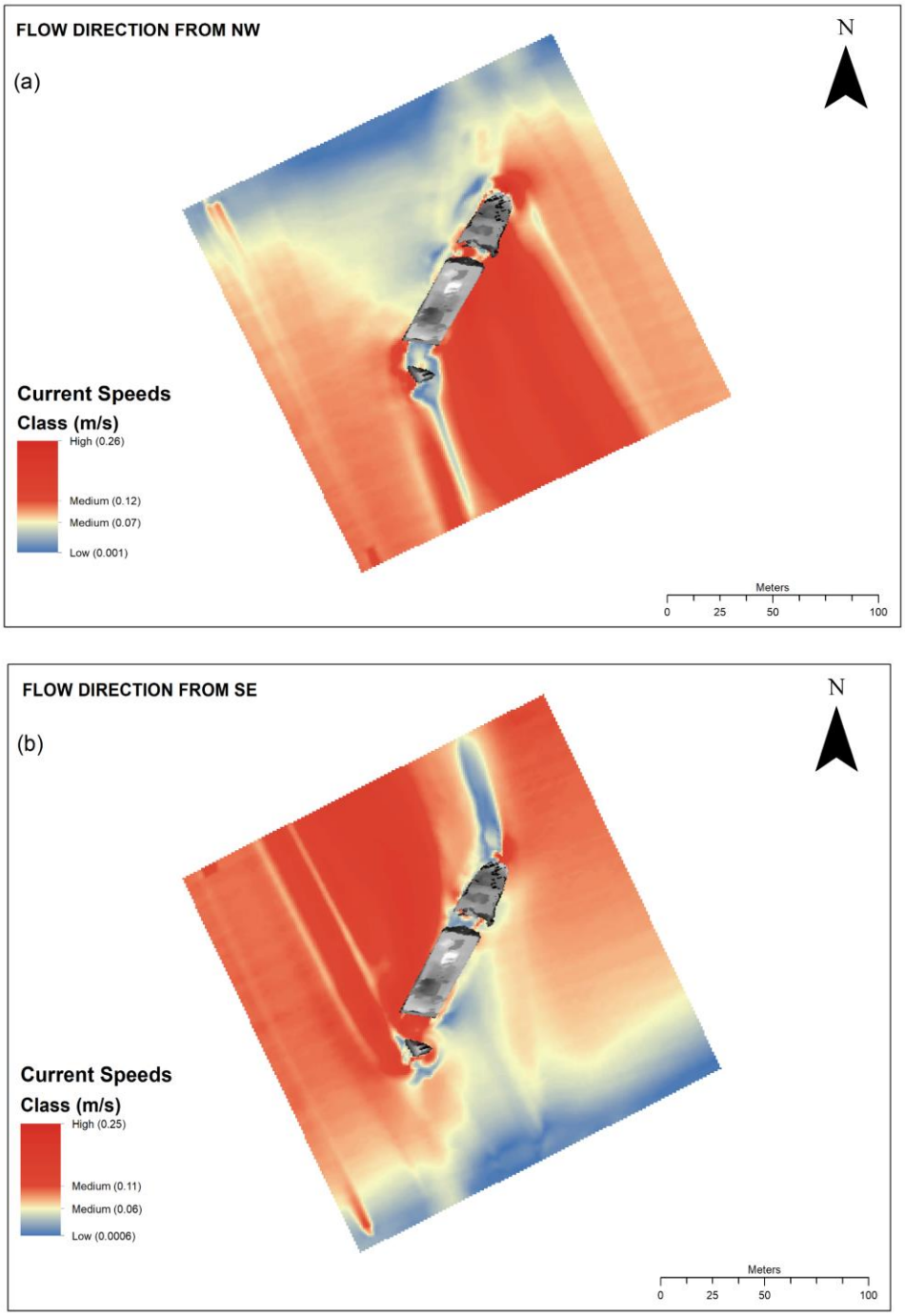

Figure 5. Maps representing current velocities close to the seabed for flow from the NW (**a**) and flow from the SE (**b**).

Flow rates from the NW were divided and categorized as low velocity (0.001–0.07 m/s), medium velocity (0.07–0.12 m/s) and high velocity (>0.12 m/s) based on the Jenks natural breaks classification of the velocity distribution. The Jenks natural breaks classification method determines the best arrangement of values into different classes by minimizing each class's average deviation from the mean, while maximizing each class's deviation from the means of the other groups [30]. Flow rates for the SE were categorized as low velocity (0.0006–0.06 m/s), medium velocity (0.06–0.11 m/s), and high velocity (>0.11 m/s).

Flow from the NW displays a large area of high velocity flow, directly in the central wake of the wreck (Figure 5a). This area is surrounded on either side by a low velocity area, wrapping itself around the wreck's bow and stern, producing a typical wake flow. The flow from the bow appears much more pronounced, flowing through the large break in the hull. Another small area of high-velocity flow emerges on the outside of the bow wake, sandwiching the lower velocity flow in between itself and the central wake. As the approach flow makes contact with the wreck on its starboard side it produces two distinct areas of low velocity: at the stern and at the break in the midsection. The areas of high and low velocity are paralleled by a mid-velocity flow on either side.

The high velocities in the flow from the SE to NW are concentrated mainly towards the bow of the wreck, pushing through the gap in the bow. The high-velocity wake is intersected by a thin stream of low velocity flow and bordered by another to the SW. A large low-velocity wake emerges from the stern, separated from the main high-velocity wake by a low-mid flow. Again, the approach flow produces areas of low velocity upon reaching the wreck directly, however they span the entirety of the wreck from bow to stern, with a small high-velocity area appearing in front of the separated bow section. A medium-velocity flow runs either side of the main wake.

Streamline models were generated in ParaView for both current directions (Figures 6 and 7), showing more complex flow velocity patterns overlaid on bed shear stress values. Flow velocity for both directions ranged from 0.0047 m/s to 0.22 m/s.

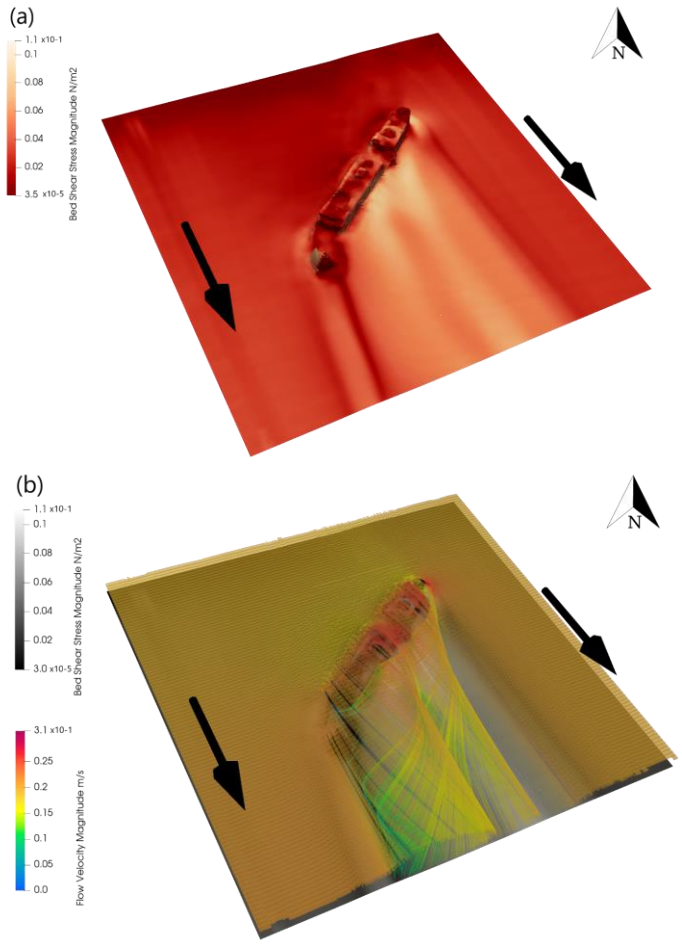

Figure 6. (**a**) Bed shear stress distribution for flow from NW to SE, brighter colors represent higher shear stress. (**b**) Streamlines represent simulated flow patterns with calculated current velocity in from NW to SE.

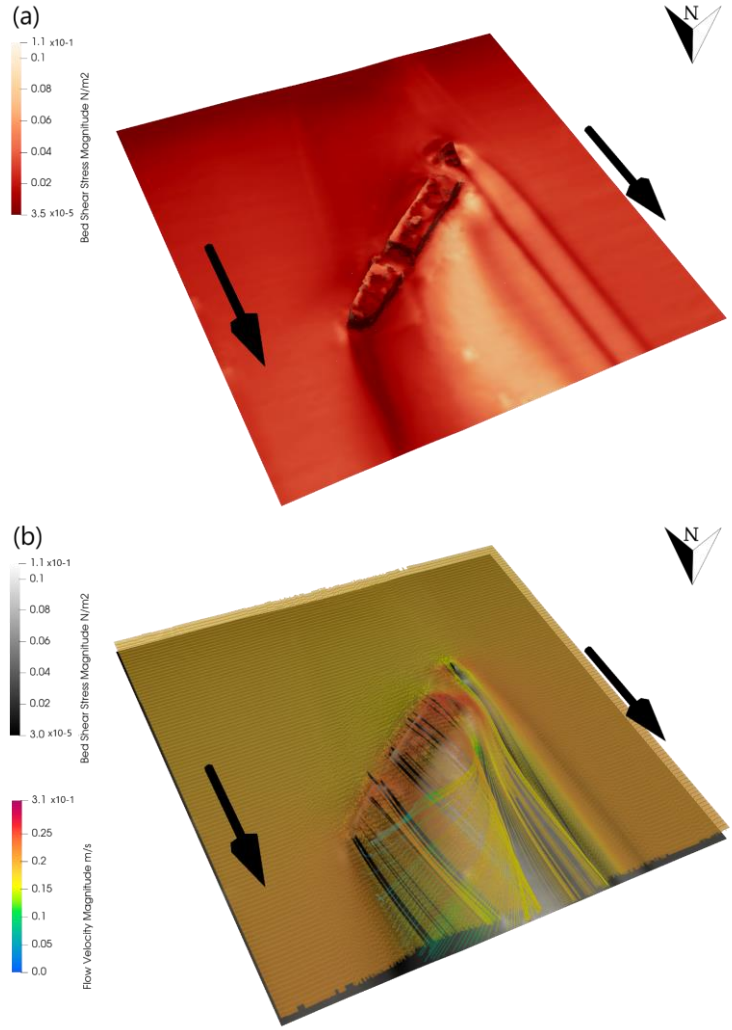

Figure 7. (**a**) Bed shear stress distribution for flow from SE to NW, brighter colors represent higher shear stress. (**b**) Streamlines represent simulated flow patterns with calculated current velocity in from SE to NW.

Figure 6 shows the flow from the NW to SE. Laminar flow is dominant either side of the bow and stern of the wreck, where shear stress is minimal. As the flow interacts directly with the wreck, however, complex patterns emerge in the wake where horizontal flow separation occurs. As water flows around the wreck's stern, it turns inward towards the wreck where two major low-velocity vortices form. These vortices occur where the bed shear stress is highest, losing rotation as they continue towards the outflow of the study area. The break towards the ship's stern appears to be a major contributing factor towards the formation of these vortices.

The SE to NW flow shows a similar pattern of vortices where it interacts with the wreck, with steady, laminar flows either side (Figure 7). Similarly, it shows the formation of two distinct vortices, through the gap in the hull towards the bow of the ship; the first, towards the east is a significantly developed, low velocity vortex stretching all the way to the stern before being contained by the surrounding flow; the second, towards the west, is a far less developed vortex, distinguished from the surrounding flow by its lower velocity and slight rotation. Again, where both vortices occur, bed shear stress is at its highest.

4.2. Bed Shear Stress

In sediment mobility studies, current speeds are converted to bed shear stress to assess the force acting on a particular sediment type [7]. In OpenFOAM, the bed (or wall) shear stress vector (τc) is calculated using the built-in wallShearStress function at selected wall

patches using the equation $\tau c = R \cdot n$, where R is shear-stress symmetric tensor retrieved from the turbulence model and n is the patch normal vector (into the domain). The resulting values are given in m^2/s^2. Using the calculator function within Paraview, we multiplied our wall shear stress values by our fluid density (seawater at 10 °C, 1027 kg/m^3) in order to give values in Pascals. Figure 8 shows bed shear stress overlaid with areas exhibiting erosional and depositional signatures defined from survey data by [1]. The flow originating from the NW displays a maximum value of 0.091 Pa and a minimum of 0.00008 Pa, with a mean of 0.03 Pa (Figure 8a). Flow from the SE displays a maximum value of 0.085 Pa and a minimum of 0.00008 Pa, with a mean of 0.026 Pa (Figure 8b). Both flow directions were also characterized separately as having areas of high, medium, and low shear stress based on natural breaks in the data distribution. Flow rates for the NW were categorized as low shear stress (0.00008–0.02 Pa), medium shear stress (0.02–0.04 Pa), and high shear stress (>0.04 Pa). Flow rates for the SE were categorized as low shear stress (0.00008–0.02 Pa), medium shear stress (0.02–0.05 Pa), and high shear stress (>0.05 Pa).

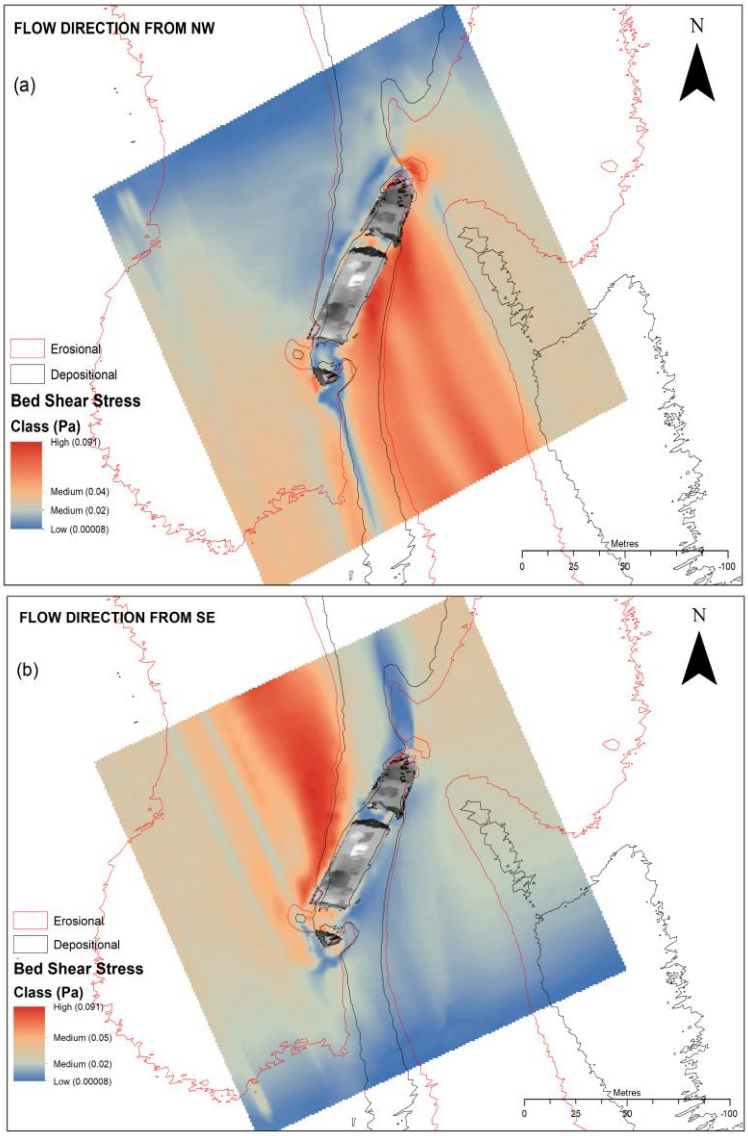

Figure 8. Maps representing bed shear stress (in Pascals (Pa) with flow from the NW (**a**) and flow from the SE (**b**). Bed shear stress values are classed as low, medium and high, as described in the text. Red and black lines represent areas of erosion and deposition, respectively, as delineated in [1] 4.3 Scalar Transport.

Flow from the NW displays a large area of high shear stress in the center of the wreck's wake, surrounded on either side by areas of low stress. Another, thin area of high stress wraps around the highly defined low stress emerging from the wake of the wreck's bow. There is a small area of high stress in the midship break and a prominent one at the point of the wreck's stern. A large area of low stress is present in the approach flow, making contact with the full length of the wreck. Areas of medium stress are present on either side of the wake.

Flow from the SE displays a large area of high stress in the wreck's wake, skewed towards the bow. Two thin lines of low stress emerge on the SW side of the high stress; one intersecting an area of medium-high stress; the other bordering it. A large, well-defined area of low stress emerges from the stern wake, with a very small area of high stress at the point of the stern and a slightly larger one in the gap between the bow and the main section. As with the NE flow, the approach flow contains a large, low stress area that makes contact along the length of the wreck.

The seabed signature patterns of erosional and depositional areas suggest a symmetry, with significant erosional areas adjacent to the wreck on the west side and the east side. A separate large area of deposition occurs to the SE, with a thin signature of low deposition slightly north. Neither of these areas show a symmetrical comparison to the NW. The areas of erosion and deposition represented by the previous survey data compare well with the areas of high and low shear stress generated from the model outputs. In the wreck's wake the boundaries outlining erosional effects follow the model predictions closely, with high shear stress in the center. The areas outside this high-stress area, where velocity and shear stress drop to low values, are outlined by areas of deposition from the survey data. The SS Polwell itself is located in a signature indicating an area of deposition, with the model outputs showing low shear stress in the vicinity of the wreck body.

Model outputs for T were exported from ParaVIEW and processed within ESRI ArcMAP to display the scalar transport parameter (T) for the NW to SE flow direction and the SE to NW flow, overlaid with scour and deposition signatures obtained from repeat survey data (Figure 9). T values ranged from 0 (least concentration of tracer element) to 1 (maximum concentration of tracer element), reflecting areas most and least associated with the transport of suspended sediment. Outputs for each flow direction were sampled at 1400 iterations to provide an accurate representation of scalar transport at developed shear stress values. T values were examined only where they interacted with the wreck.

The NW to SE flow for scalar transport (Figure 9a) shows a significant area of transport in the wreck's wake, from the bow to the southernmost break in the hull. At the bow itself (NE section of the wreck), a high level of transport wraps around from the approach flow side to join and extend the transport travelling in a south-southeast (SSE) direction. From the northmost break on the approach flow side, an area of medium to high transport (around 0.6 to 0.8) follows the length of the wreck to the stern then travels in a direction orientated SSE, in a separate flow parallel to the largest, most significant flow and dissipates as it reaches the edge of the area. Immediately south of the stern shows an area of low transport, surrounded by the two large high transport areas. This low transport appears to continue south, splitting the two larger flows and becoming more prominent at the southernmost edge of the modelled area. The breaks themselves both show a medium to high level of transport.

The SE to NW flow for scalar transport (Figure 9b) shows its most significant transport taking place directly in the wreck's wake. The wake transport can be divided into two individual sections. The first and largest area of transport, from the wreck's stern to the southern break, consists of medium transport directly in its wake increasing to high to the northeast towards the edge of the area. The second area begins concentrated on the broken section of bow, at the southern tip of the wreck. This high level of transport encompasses the broken piece of hull and stretches out to the northwest, parallel to the larger area in the wake. A strip of medium to high flow stretches from one hull break to the other where the

approach flow meets the wreck. The break towards the stern section displays low levels of transport.

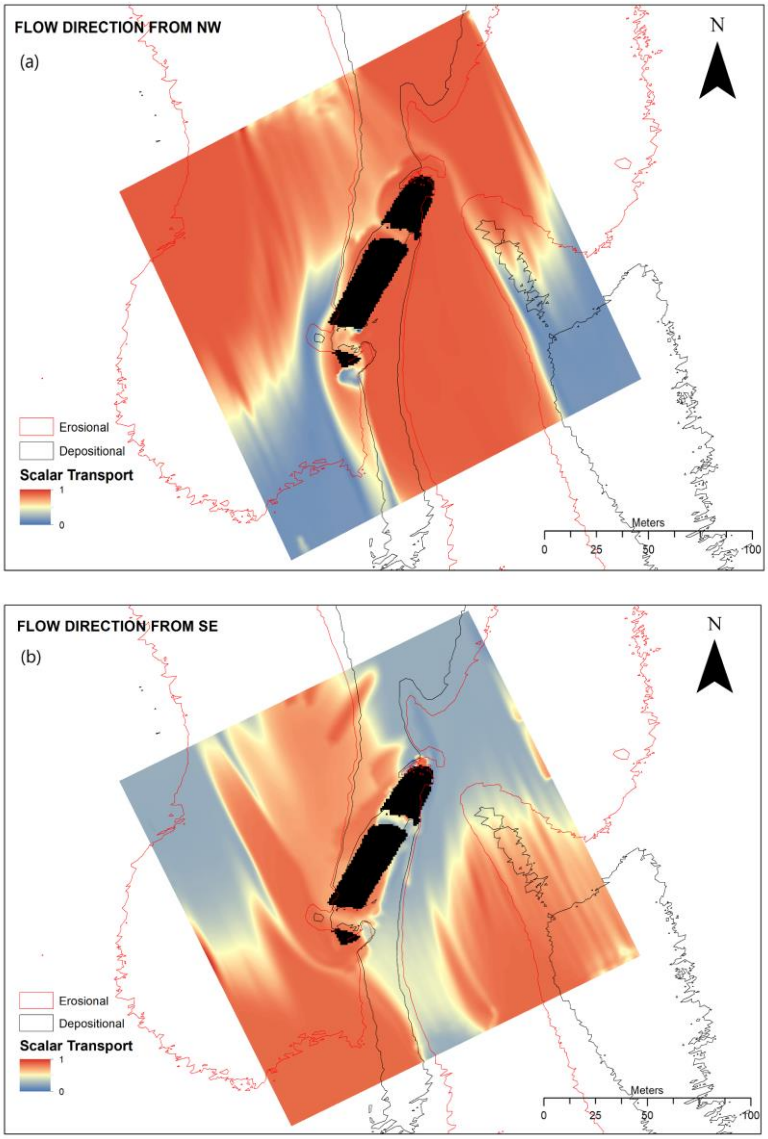

Figure 9. Map representing scalar transport concentrations with erosional and depositional signatures for the NW to SE flow (**a**), and SE to NW flow (**b**).

5. Discussion

5.1. CFD Model Simulations and Comparisons with Repeat Survey Data

The results from this study suggest that, despite a complex interaction of hydrodynamics with a seabed obstacle (i.e., a shipwreck), CFD modelling is capable of producing outputs that can be qualified using real-world survey data to explain seabed sediment dynamics. Previous studies have sought to understand seabed hydrodynamics and scour through the sole use of repeat surveys or in situ monitoring devices, or a combination of both [1,20]. By examining a summation of survey data, velocity values, shear stress, and flow regimes we have created a multidimensional, multipurpose model.

Examination of the current velocity shows a typical flow pattern in the wreck's wake where pressure gradients created by flow around and over the wreck result in increased velocity in the center of the wake, with less energetic flows on either side [17]. The median values of 0.1305 m/s for the NW flow, and 0.1253 m/s for the SE flow, reflect the slightly higher current velocities from the NW. Velocity values in the immediate vicinity of the

wreck, excluding the wake areas, show an amplification of velocity when compared to the mean depth averaged velocity of 0.147 m/s. Flow from the NW to SE shows an amplification factor of 2, as does flow from the SE to NW. This broadly agrees with findings from Smyth and Quinn [17] and Whitehouse [7], where they highlight that flow is amplified by the presence of a wreck or obstacle, including the immediate wake, by a factor of 3 to 4: an order higher than those presented here.

The patterns of velocity correspond well to the patterns of shear stress, creating near-mirror images. The patterns of shear stress suggest an area of erosion in the center of the wreck's wake, with deposition on either side and where the approach flow contacts the wreck itself. This is supported by the previous survey data overlaid, showing areas of erosion and deposition by examining changes in depth. These patterns of velocity and shear stress correlate well with the overlaid survey data in that where high shear stress occurs erosion takes place, and where low shear stress occurs, deposition takes place. The scalar transport also corresponds closely to the bed shear stress, suggesting a coupling of high shear stress to higher levels of sediment transport. Areas of sediment erosion observed in the repeat survey data appear to correlate well with areas of high transport in the CFD model, as do areas of deposition with low transport values.

It is known, however, from temporal comparison of repeat survey data that the SS Polwell and the area adjacent do not show any signs of significant scour, typically −0.02 to −0.04 m on an interannual basis, instead suggesting a slight tendency towards deposition [20]. This is probably due to a combination of factors. Current speed in the area is considered to be relatively low in the area when compared to other shipwreck sites examined by Majcher et al. [1] (e.g., SS Hare, SS Tiberia). With less energetic currents in the area on average throughout the year, combined with too great a depth for the wave base to interact with the seabed, the mobilization of sediment is less likely to occur. Additionally, the presence of diurnal tides of equal magnitude would work to, at least partially, negate the mass transport of sediment outside the immediate area. The SS Polwell lies in a multimodal sediment, composed of gravelly muddy sand, with muddy sand further out (Figure 1). This could have contributed to the lack of scour in that the finer mud has already been transported, or winnowed, from the area, leaving the coarser grains behind as a lag. This gravelly, muddy sand would require a higher threshold of mobilization when compared to finer mud or sand.

When examined closely, the flow patterns of the streamline models produced in OpenFOAM show that the vortices produced in the high areas of shear stress in the wreck's wake, are actually lower in velocity than the current close to the seabed. This suggests that rather than working to transport suspended sediment out of the system, the vortices enable suspension of the sediment in place. The higher velocities may exceed the mobilisation threshold, lifting the sediment into the vortex where the lower velocity cause it to dip back below the threshold, effectively resettling sediment back into to the seabed where it is lifted from again, creating a cycle until slack water signals reversal of the flow and temporarily interrupts the cycle.

When the scalar transport is examined for the NW to SE flow (Figure 9a), areas of high shear stress appear to correlate well with higher values for T. After making contact with the wreck, the scalar transport displays a horseshoe pattern in its wake, suggesting a higher transport potential for sediment within the secondary flows created by the perturbed approach flow. The bounds of the transport areas appear duplicated in the bed shear stress model, with a line of low shear stress and transport both shown flanking the main middle high value area on both sides. In particular, a lesser transport flow occurs immediately southwest of this line, showing great similarity to the shear stress model. The SE to NW flow (Figure 9b) repeats these patterns, with a higher value region originating from the wreck's bow in terms of both scalar transport and shear stress. Transport over the wreck appears more intense for the NW to SE flow. While it is mainly concentrated from the stern to the southernmost break, it suggests the potential for sediment to be transported over the wreck from both the approach flow area and the deposited sediment on the approach side

shown in the repeat survey data. The SE to NW flow also shows this potential for transport over the wreck, albeit switched around, with the higher areas stemming from the bow as opposed to the stern.

5.2. Limitations and Recommended Further Work

The domain size of the study area sampled may not be sufficiently large to fully resolve the dynamic nature of the regional area. The inlet approach in particular may not allow for full development of the flow before reaching the SS Polwell. For example, to the north of the wreck site lies a pipeline in a roughly west to east orientation, and to the south lies an area of complex bedforms, both of which may further complicate the flow regime by introducing further obstructions to perturb tidal currents (Figure 1). The high-resolution nature of the input bathymetry data meant that CFD simulations for a larger area incorporating these features would require too much computer processing power in the context of this study. In order to better constrain inlet conditions for the high-resolution model domain of the immediate wreck site and generate more realistic flow simulations, a coarser-resolution model could be developed initially for a larger domain area in the up- and downstream directions of tidal current flow. This model would capture regional flow patterns and the outputs could be used as input along the boundary of the smaller, high-resolution model [22].

For the purposes of this study, the steady-state solver SimpleFOAM was employed as the focus specifically was on verification of a CFD model using data taken from a single survey (4–10 October 2019). However, seabed sediment dynamics, and in particular scour development, can evolve significantly over time and so require transient solvers [16,17]. At the SS Polwell site there is repeat bathymetric survey data that would allow for assessment of geomorphic change over varying temporal timescales, ranging from 1 week to 1 year to 4 years. Detailed analysis of these temporal changes would require a large-scale transient solver such as PimpleFOAM in order to provide an in-depth analysis of scour evolution over time.

The result of CFD can be used in calculating sediment mobility levels using grain-size properties of sediment samples [22]. However, the multimodal nature of sediment at the seafloor of the SS Polwell site represents a complex geological setting in terms of sediment distribution (Figure 1). As a result, no single value for the threshold of movement can be applied to the site to determine sediment mobility, making it difficult to calculate net movement of sediment and precise levels of scour or deposition. The transport equation integrated into the solver in this study does not account for sediment size, but instead uses a dimensionless 'tracer', designed to represent a generic transport value applied to sediment already in motion and, as such, does not take into account mobilization values. Instead, shear stress values represent areas where sediment mobilization is most/least likely to occur. The mobilization of the sediment particles is governed by the Shields parameter:

$$\tau^* = \tau/(ps - p)\,gD \quad (4)$$

where τ is the dimensional shear stress, ps is sediment density, p is the fluid density, g is the gravitational acceleration and D is the particle diameter of the sediment.

Pang et al. [31] demonstrated a critical Shields value that corresponds with the equilibrium scour depth. Previously, [1] utilized regionally modelled current speed data from the Marine Institute ROMS-based model to calculate exceedance values for sediment types at differing shipwreck sites. As highlighted in this study, values for current speed across a site with an obstacle (i.e., a shipwreck) can vary considerably depending on amplification factors associated with that obstacle, as well as seabed morphology. In this instance, current velocities were increased two-fold in the immediate vicinity of the wreck. Using more detailed current speed and calculated bed-stress data outputs from the model developed in this study, in conjunction with a sediment grain-size database and the scalar transport model, would allow for a much more robust assessment of sediment mobility due to threshold exceedance.

The Integrated Mapping for the Sustainable Development of Ireland's Marine Resource (INFOMAR) programme has been mapping the Irish seabed since 2006, and in that time has mapped some 457 shipwrecks in varying degrees of detail. The quality of this database, and its broad geographic extent, means that the approach described here can be applied to a significant number of other sites in the Irish territory in differing hydrodynamic and seabed morphological and sedimentary settings. A future examination of multiple seabed obstructions and/or morphology types and their effects on the overall flow regime in this manner could serve to elucidate the complex nature of obstacle induced hydrodynamic flow and scour development, allowing for an extensive, regional assessment of scour potential.

6. Conclusions

This study used high-resolution models from bathymetric survey data to create inputs in CFD simulations in OpenFOAM software. In turn, these simulations were used to study the complex interactions between seafloor hydrodynamics and seabed objects, allowing us to explain geomorphic change through patterns of erosion and deposition compared to temporal bathymetric data for the same site. Modelled outputs for current flow and stress patterns correspond well with known seabed signatures for sediment erosion and deposition from survey data. In addition, t scalar transport equations were solved to determine sediment movement patterns once grains were mobilized. This study demonstrates that this integrated methodology can be used to predict scour and sediment mobility patterns at seabed objects; in this case, a shipwreck site. The outputs from this approach can also be used in conjunction with repeat and physical (i.e., grab sample) survey data in order to understand temporal sediment dynamics and morphological change at a localized level. Ultimately, this approach can be adapted and applied to other man-made structures (such as offshore wind turbine foundation structures) on the seabed as part of engineering design studies to mitigate against the risk of scour causing instability.

Author Contributions: Conceptualization, J.K. and M.C.; methodology, J.K. and M.C; software, G.L.; validation, G.L., formal analysis, G.L. and J.M.; investigation, G.L.; resources, G.L.; data curation, G.L.; writing—original draft preparation, G.L.; writing—review and editing, J.K. and M.C.; visualization, G.L. and J.M.; supervision, J.K. and M.C.; project administration, J.K.; funding acquisition, M.C. and J.K. All authors have read and agreed to the published version of the manuscript.

Funding: This research was funded by Geological Survey Ireland, grant number 2020-SC-001.

Data Availability Statement: Not applicable.

Acknowledgments: This project is funded by the Geological Survey of Ireland (GSI) Geoscience Research Programme under their 2020 Short Calls. Acquisition of bathymetry data was supported by the Marine Institute of Ireland's ship-time programme's APP-CV15021, CV16031: World War I shipwrecks in the Irish Sea: commemoration, visualization and heritage management and APP-CV19027: Geohazard investigation in the Irish Sea using seismic and seabed mapping techniques (GIST). The authors thank the crew of the RV Celtic Voyager on these surveys for their skill and dedication, as well as Rory Quinn, Ruth Plets, Chris McGonigle, Kieran Westley and Fabio Sacchetti for provision of data and support. The authors also express their gratitude to the MI Oceanographic Services Team for their support with ocean current data requests. Jan Majcher is supported by an Ulster University Vice-Chancellor's Research Studentship. MC is funded under an Irish Research Council Enterprise Partnership Scheme Postdoctoral Fellowship (EPSPD/2020/109) and in part by a research grant from Science Foundation Ireland (SFI) under Grant Number 13/RC/2092, with support from Gavin and Doherty Geosolutions Ltd and the Geological Survey of Ireland (GSI). The authors would like to thank the reviewers for their suggestions and comments, which provided valuable insight and improvement of the paper to the highest standard.

Conflicts of Interest: The authors declare no conflict of interest. The funders had no role in the design of the study; in the collection, analyses, or interpretation of data; in the writing of the manuscript; or in the decision to publish the results.

References

1. Majcher, J.; Quinn, R.; Plets, R.; Coughlan, M.; McGonigle, C.; Sacchetti, F.; Westley, K. Spatial and temporal variability in geomorphic change at tidally influenced shipwreck sites: The use of time-lapse multibeam data for the assessment of site formation processes. *Geoarchaeology* **2021**, *36*, 429–454. [CrossRef]
2. Mellet, C.; Long, D.; Carter, G.; Chiverrell, R.; van Landeghem, K. *Geology of the Seabed and Shallow Subsurface: The Irish Sea*; British Geological Survey: Edinburgh, UK, 2015.
3. Quinn, R.; Bull, J.; Dix, J. Buried scour marks as indicators of palaeo-current direction at the Mary Rose wreck site. *Mar. Geol.* **1997**, *140*, 405–413. [CrossRef]
4. Bauri, K.P.; Sarkar, A. Flow and scour around vertical submerged structures. *Sādhanā* **2016**, *41*, 1039–1053. [CrossRef]
5. Schendel, A. Wave-Current-Induced Scouring Processes and Protection by Widely Graded Material. Ph.D. Thesis, Institutionelles Repositorium der Leibniz Universität Hannover, Hannover, Germany, 2018.
6. Okayasu, A.; Fujii, K.; Isobe, M. Effect of external turbulence on sediment pickup rate. *Coast. Eng. Proc.* **2011**, *1*, 14. [CrossRef]
7. Whitehouse, R. *Scour at Marine Structures*; Thomas Telford Services Ltd.: London, UK, 1998.
8. De Vos, L.; De Rouck, J.; Troch, P.; Frigaard, P. Empirical design of scour protections around monopile foundations: Part 1: Static approach. *Coast. Eng.* **2011**, *58*, 540–553. [CrossRef]
9. De Vos, L.; De Rouck, J.; Troch, P.; Frigaard, P. Empirical design of scour protections around monopile foundations. Part 2: Dynamic approach. *Coast. Eng.* **2012**, *60*, 286–298. [CrossRef]
10. Ma, H.; Chen, C. Scour protection assessment of monopile foundation design for offshore wind turbines. *Ocean Eng.* **2021**, *231*, 109083. [CrossRef]
11. Whitehouse, R.; Sutherland, J.; Harris, J. Evaluating scour at marine gravity foundations. *Proc. Inst. Civ. Eng.-Marit. Eng.* **2011**, *164*, 143–157. [CrossRef]
12. Matutano, C.; Negro, V.; López-Gutiérrez, J.-S.; Esteban, M.D. Scour prediction and scour protections in offshore wind farms. *Renew. Energy* **2013**, *57*, 358–365. [CrossRef]
13. Whitehouse, R.J.S.; Harris, J.M.; Sutherland, J.; Rees, J. The nature of scour development and scour protection at offshore windfarm foundations. *Mar. Pollut. Bull.* **2011**, *62*, 73–88. [CrossRef]
14. Welzel, M.; Schendel, A.; Hildebrandt, A.; Schlurmann, T. Scour development around a jacket structure in combined waves and current conditions compared to monopile foundations. *Coast. Eng.* **2019**, *152*, 103515. [CrossRef]
15. Li, Y.; Ong, M.C.; Fuhrman, D.R.; Larsen, B.E. Numerical investigation of wave-plus-current induced scour beneath two submarine pipelines in tandem. *Coast. Eng.* **2019**, *156*, 103619. [CrossRef]
16. Smyth, T.; Quinn, R. The role of computational fluid dynamics in understanding shipwreck site formation processes. *J. Archaeol. Sci.* **2014**, *45*, 220–225. [CrossRef]
17. Quinn, R.; Smyth, T. Processes and patterns of flow, erosion, and deposition at shipwreck sites: A computational fluid dynamic simulation. *Archaeol. Anthropol. Sci.* **2018**, *10*, 1429–1442. [CrossRef]
18. Fernández-Montblanc, T.; Izquierdo, A.; Quinn, R.; Bethencourt, M. Waves and wrecks: A computational fluid dynamic study in an underwater archaeological site. *Ocean Eng.* **2018**, *163*, 232–250. [CrossRef]
19. Yang, B.; Wei, K.; Yang, W.; Li, T.; Qin, B. A feasibility study of reducing scour around monopile foundation using a tidal current turbine. *Ocean Eng.* **2020**, *220*, 108396. [CrossRef]
20. Majcher, J.; Plets, R.; Quinn, R. Residual relief modelling: Digital elevation enhancement for shipwreck site characterisation. *Archaeol. Anthr. Sci.* **2020**, *12*, 122. [CrossRef]
21. Calder, B.; Wells, D. CUBE User's Manual. Durham: University of New Hampshire. Available online: http://ccom.unh.edu/sites/default/files/publications/Calder_07_CUBE_User_Manual.pdf (accessed on 1 October 2021).
22. Majcher, J.; Quinn, R.; Smyth, T.; Plets, R.; McGonigle, C.; Westley, K.; Sacchetti, F.; Coughlan, M. Using difference modelling and computational fluid dynamics to investigate the evolution of complex, tidally influenced shipwreck sites. *Ocean Eng.* **2022**, *246*, 110625. [CrossRef]
23. Yu, H.; Thé, J. Validation and optimization of SST k-ω turbulence model for pollutant dispersion within a building array. *Atmospheric Environ.* **2016**, *145*, 225–238. [CrossRef]
24. Franke, J.; Hellsten, A.; Schlunzen, K.H.; Carissimo, B. The COST 732 Best Practice Guideline for CFD simulation of flows in the urban environment: A summary. *Int. J. Environ. Pollut.* **2011**, *44*, 419. [CrossRef]
25. Mo, J.-O.; Choudhry, A.; Arjomandi, M.; Kelso, R.; Lee, Y.-H. Effects of wind speed changes on wake instability of a wind turbine in a virtual wind tunnel using large eddy simulation. *J. Wind Eng. Ind. Aerodyn.* **2013**, *117*, 38–56. [CrossRef]
26. Soulsby, R. *Dynamics of Marine Sands*; Thomas Telford: London, UK, 1997.
27. Lewis, M.; Neill, S.; Robins, P.; Hashemi, M.; Ward, S. Characteristics of the velocity profile at tidal-stream energy sites. *Renew. Energy* **2017**, *114*, 258–272. [CrossRef]
28. Nagy, H.; Lyons, K.; Nolan, G.; Cure, M.; Dabrowski, T. A Regional Operational Model for the North East Atlantic: Model Configuration and Validation. *J. Mar. Sci. Eng.* **2020**, *8*, 673. [CrossRef]
29. Shchepetkin, A.F.; McWilliams, J.C. The regional oceanic modeling system (ROMS): A split-explicit, free-surface, topography-following-coordinate oceanic model. *Ocean Model.* **2005**, *9*, 347–404. [CrossRef]

30. Chen, J.; Yang, S.T.; Li, H.W.; Zhang, B.; Lv, J.R. Research on geographical environment unit division based on the method of natural breaks (Jenks). *Remote Sens. Spat. Inf. Sci.* **2013**, *4*, 47–50. [CrossRef]
31. Pang, A.; Skote, M.; Lim, S.; Gullman-Strand, J.; Morgan, N. A numerical approach for determining equilibrium scour depth around a mono-pile due to steady currents. *Appl. Ocean Res.* **2016**, *57*, 114–124. [CrossRef]